Electronic Supplementary Material (ESI) for Nanoscale.
This journal is © The Royal Society of Chemistry 2016

Flexible infrared detectors based on *p-n* junctions of muti-walled carbon nanotubes

Supporting information

S1. Growth of the non-doped CNTs and nitrogen doped CNTs by floating catalyst CVD method.

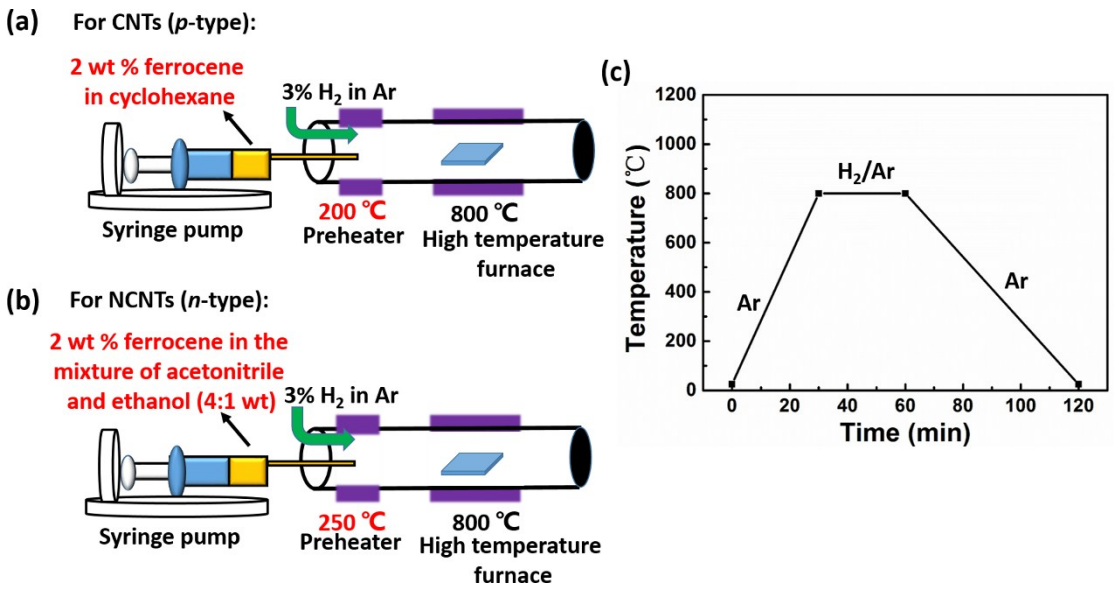

Fig. S1 Schematic of the floating catalyst CVD setup. (a) Growth of non-doped CNTs (*p*-type). (b) Growth of nitrogen doped CNTs (*n*-type). (c) Temperature control of the furnace.

S2. Raman spectra of CNTs and NCNTs.

Fig. S2 shows the Raman spectra of undoped CNTs and nitrogen-doped CNTs (NCNTs). For the two kinds of specimens, the Raman spectra were measured under the same conditions. Undoped CNTs possess a D band (around 1339.3 cm^{-1}) and G band (around 1570.8 cm^{-1}), and the intensity ratio of G band/D band (I_G/I_D) is 1.52.

Compared with undoped CNTs, the value of I_G/I_D for NCNTs decrease to 1.12, indicating that nitrogen doping has introduced some defects into the structure of the CNTs. Besides, upon nitrogen doping, the D band upshifts from 1339.3 cm^{-1} to 1346.8 cm^{-1}, which is own to the appearance of new types of disorder in CN_x nanotubes.[1,2]

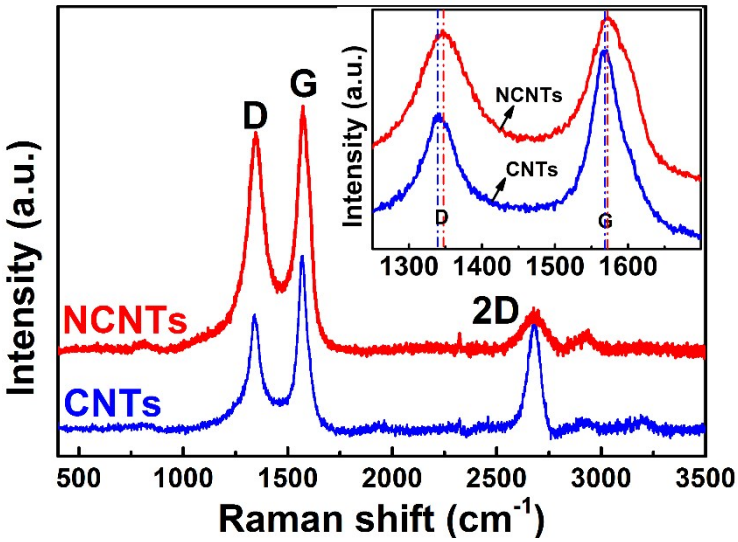

Fig. S2 Raman spectra of CNTs (blue line) and NCNTs (red line).

S3. Field effect transistors based on muti-walled (N)CNTs.

To explore the semiconductor properties of the two kinds of CNTs, muti-walled CNTs-based field effect transistors (FET) were fabricated and the performances of the devices are shown in Fig. S3. Fig. S3a shows the structures of the FET devices. To get the device, the CNTs solution was prepared first: 0.01g CNTs was put into 40 ml N-methyl pyrrolidone, followed by ultrasonic dispersion and centrifugation. Then a layer of CNTs film was deposited on the surface of the SiO_2/Si (thickness: 300nm/500um) by spray method.[3] The source and drain electrodes were Au/Ni (thickness: 120nm/60nm), which were fabricated by magnetron sputtering. Fig. S3b shows the SEM top view image of the FET device and the channel width is 10 μm. Fig. S3c shows

the output characteristics I_{ds}-V_{ds} of the FET device consisting of undoped CNTs under different gate voltages. With the gate voltage V_g decreased from -10 V to -100 V, the resistance dropped quickly, indicating a controllable transition between the quasimetallic and the insulating states of the CNTs. Fig. S3d shows the transfer performance I_{ds}-V_g of the undoped CNTs based FET device at various V_{ds} from -10 mV to -100 mV. Inset of Fig. S3d gives the change of I_g vs V_g, indicating the device have little leakage even at very large bias voltage. The performance of the device shown in Fig. S3d is similar to that of *p*-channel FET.[4-6] The source-drain current Ids decreases quickly with the increase of gate voltage V_g, which means the main carrier of undoped CNTs is holes. Fig. S3e shows the performance comparison of the two kinds of FET based on undoped CNTs or nitrogen-doped CNTs (NCNTs). It can be seen that the source-drain current Ids increases with the increase of gate voltage V_g for NCNTs, which is quite different form the one based on undoped CNTs. The FET devices based on these two kinds of CNTs can give a powerful evidence to prove that the undoped CNTs present *p*-type semiconductor property and NCNTs present *n*-type semiconductor property.

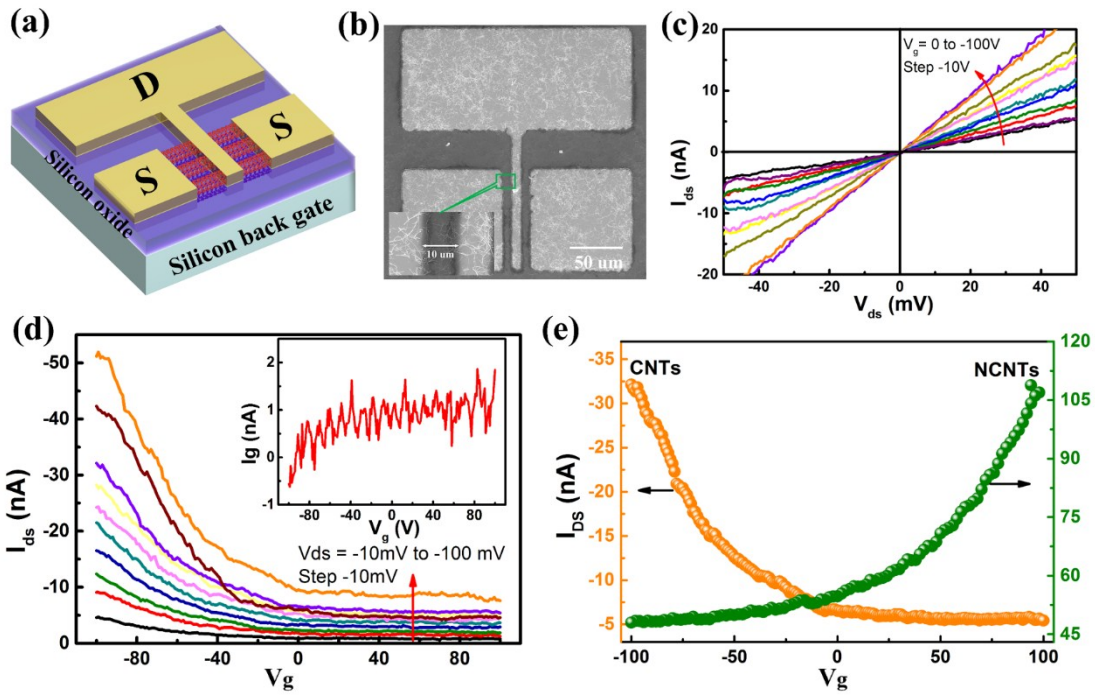

Fig. S3 (a) Structure of the FET device. (b) SEM top view of the FET device. (c) and (d) output and transfer characteristics of the undoped CNTs based FET; (c) I_{ds}-V_{ds} curves measured for V_g = 0 to -100 V in steps of -10 V; (d) I_{ds}-V_g curves for V_{ds} = -10 mV to -100 mV in steps of -10 mV, the inset shows the electric leakage I_g with different gate voltages V_g. (e) The different performance of CNTs and NCNTs based FET devices.

S4. The absorbance spectra of CNTs and NCNTs.

Fig. S4 shows the photo absorbance of both CNTs and NCNTs with photo wavelength from 260 nm to 7000 nm. And both the Fourier transform infrared (FTIR) absorbance spectra and UV-vis-NIR spectra were used to get the spectral response of these two materials. The wavelength tested by UV-vis-NIR is from 260 nm to 1100 nm and tested by FTIR is from 1000 nm to 7000 nm. From the results we can get the

conclusion that both CNTs and NCNTs demonstrated photo absorption in the wavelength range of 260 nm to 7000 nm. There are two distinct absorbance peaks located at wavelengths of 2919 nm and 6114 nm, or 3426 cm^{-1} and 1635 cm^{-1}. The absorbance peak at 2919 nm is attributed to hydrogen bonded -OH groups and absorbance peak at 6114 nm is attributed to C=C groups of CNTs.[7]

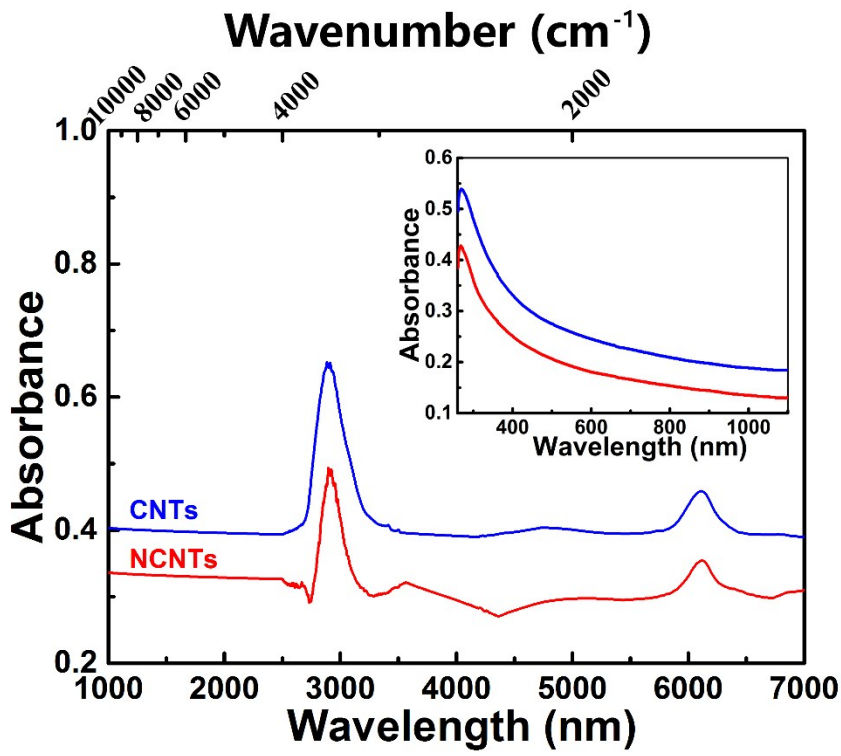

Fig. S4 FTIR and UV-vis absorbance spectra of CNTs and NCNTs.

S5. The influence of metallic CNTs for the I-V curve of the detector.

CNT can be metallic or semiconducting, depending on defect, doping and chirality of the CNT structure. CNT arrays grown from CVD method contain both of these two kinds of CNTs.[8, 9] So when We use the arrays to build *p-n* junction, there are two parallel ways for the electric carriers to get through the junction, as shown in Fig. S5a. One is the *p-n* junction constructed by the *p*-type semiconducting CNT and *n*-type

semiconducting CNT. Another is pure resistance constructed by metallic CNT. The equivalent circuit of this structure is shown in Fig. S5b. The metallic CNT is more conductive than the semiconducting CNT and the concentration of metallic CNTs usually is higher than the semiconducting CNTs for muti-walled CNT arrays. So most of the electric carriers can get through the metallic CNTs, even if the semiconducting CNT based *p-n* junction is closed. For the reason discussed above, there no rectification for the CNT arrays based *p-n* junction.

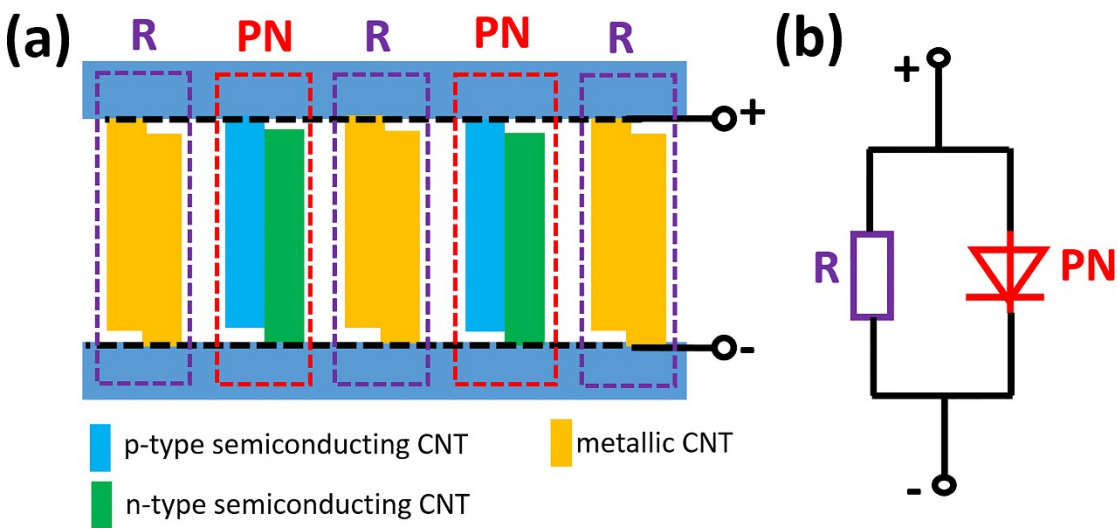

Fig. S5 (a) Sketch map showing the interlock of the CNT arrays based *p-n* junction. (b) Equivalent circuit of the CNT arrays based *p-n* junction.

S6. The influence of the IR focused position for only *p*-type or *n*-type CNT based detector.

For detector based on *p*-type only or *n*-type only, the structure of the detector is completely symmetrical, which is different from *p-n* junction based detector. The voltage difference between the two electrodes is used as the response of IR. For

symmetrical structure, when the IR focused position becomes more and more centered, the voltage difference between the two electrodes should be less and less. Take only *p*-type CNT based IR detector for example, we make the IR focus onto three different places of the detector respectively. The different positions of the focused areas are shown in inset of the Fig. S6: 1 is the position that radiation was focused on the silver electrode; 2 is the position that radiation was focused on the CNTs directly, but not in the middle of the device; 3 the position that radiation was is focused on the CNTs in the middle of the device. The periodic on/off IR radiation was focused onto the three different positions, respectively, with the same power density of 0.32 $mW.mm^{-2}$ and voltage difference between the two electrodes were recorded, as shown in Fig. S6. The black curve shows the response of the *p*-type only detector with periodic IR radiation focused on the electrode (position 1) and the photo voltage is the biggest among these three situation. When the IR radiation moved toward the middle and focused onto CNTs (position 2), the amplitude of the response decreased to 3.8 uV, as the blue curve shows. More extremely, when the IR radiation was focused onto the middle of the device (position 3), we even cannot get the response of the detector, as the red curve shows. Because potential change of the two sides is the same when the IR radiation focused on the middle of the symmetrical device, so voltage difference between the two electrodes will be zero.

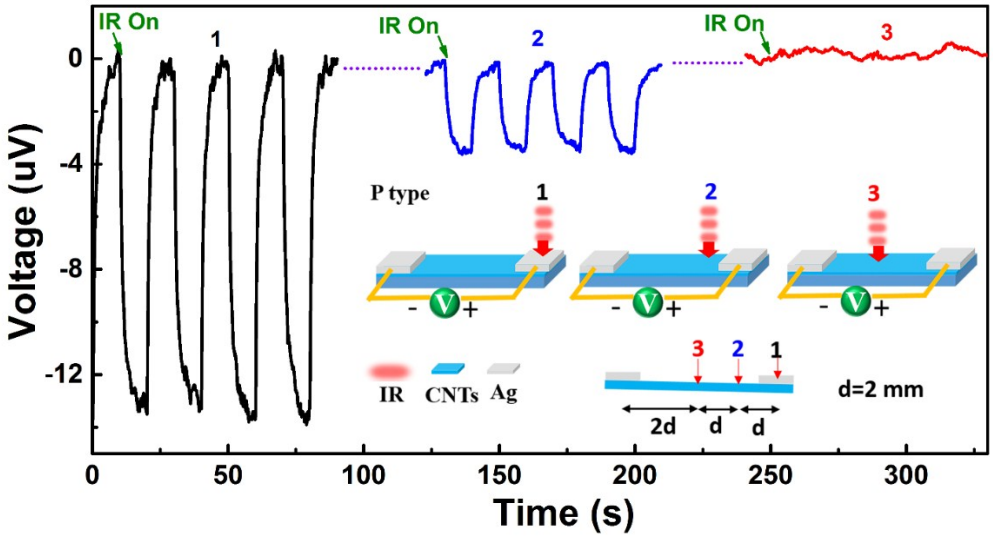

Fig. S6 Infrared response for *p*-type only CNTs based detector when the IR radiation focus on different position of the device.

S7. Exponential rise and fall behaviors with the on/off IR radiation.

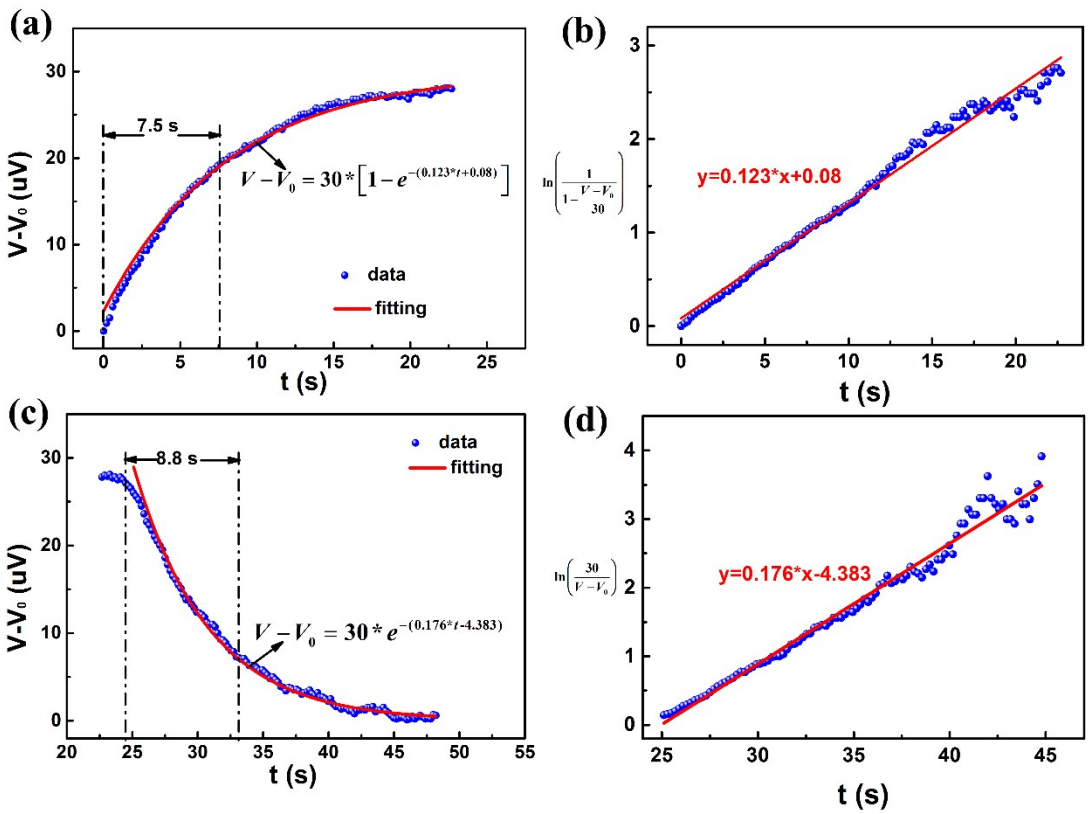

Fig. S7 The voltage response to (a) turning on and (c) turning off of the IR, showing

exponential rise and fall behaviors with the time. To present the exponential rule more clearly, the function of voltage versus time was transferred into linear relationship, as shown in Fig. S7 (b) (turn on) and (d) (turn off).

S8. Method to calculate the responsivity and detectivity of the detector.

The responsivity R_V was calculated by equation S1:

$$R_V = \frac{V}{P} \tag{S1}$$

where V is the response voltage amplitude and P is the corresponding IR power. The detection limit of photodetector is specified by the noise equivalent power (*NEP*), which is the incident power at which the signal is equal to the dark noise density (V_n). NEP can be calculated by equation S2:

$$NEP = \frac{P}{\frac{V}{V_n}} = \frac{V_n}{R_V} \tag{S2}$$

The noise V_n in our experiment is about 6×10^{-7} V and responsivity R_V is 1.05×10^{-2} V/W (without bending). Thus we can know the $NEP = 5.7\times10^{-5}$ W. Then we use the equation S3 to calculate the specific detectivity (D^*):

$$D^* = \frac{\sqrt{A\times\Delta f}}{NEP} \tag{S3}$$

where A is the area of the detector, Δf is the working bandwidth and *NEP* is the noise equivalent power. The sensing area is 27 mm^2 (considering the whole area of the device), bandwidth is 0.02 Hz and *NEP* is 5.7×10^{-5} W. Thus we know $D^* = 1.289\times10^{3}$ cm $Hz^{1/2}$ W^{-1}.

S9. Performance of the IR detector at the on/off IR radiation with on-off period of 5 s.

The base line of the IR response increased first and tended to be stable after several seconds.

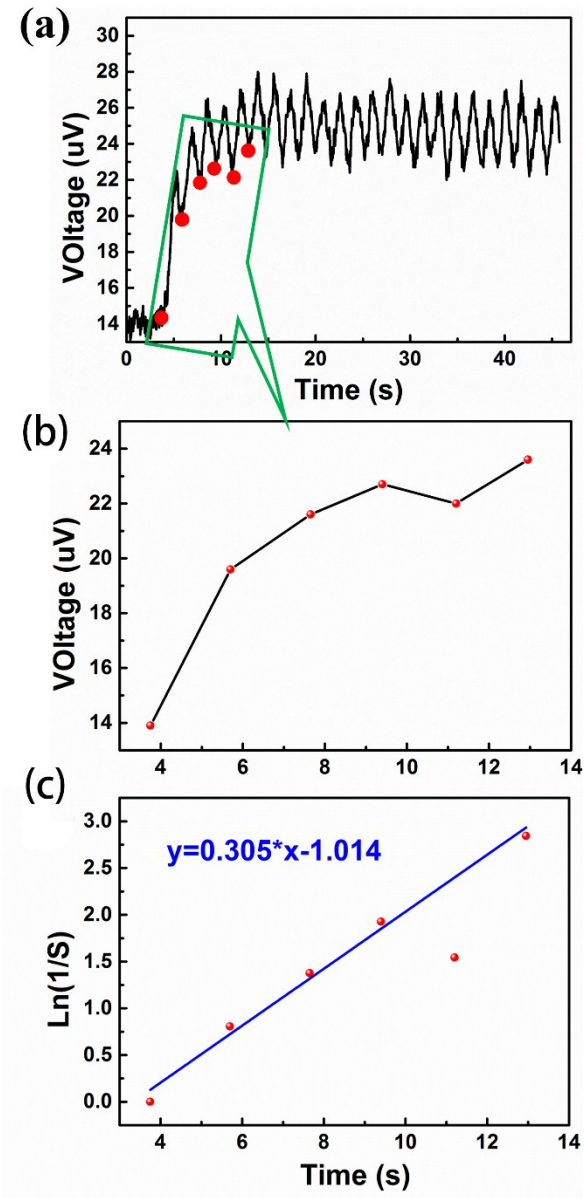

Fig. S9 IR response of the detector at the on/off IR radiation with period of 5 s. (a) Voltage of the detector versus time. (b) Base line of the voltage as a function of time.

(c) Linear fitting of ln(1/s) with time. The definition of ln(1/s) is shown in equation (3).

The base line voltage $V_b(t)$ (red point in Fig. S9 (a) and (b) change with time can be described by the following equation:

$$Vb(t) = V_{b0} + \Delta V_b \times [1 - e^{-(t-t_0)/\tau}] \tag{S4}$$

where ΔV_b is the difference between the balanced base line voltage and the original base line voltage Vb_0, t is the time, t_0 is the started time (IR on), τ is the parameter which is concerned with the thermal environment of the detectors.

Equation S4 can also be written as:

$$\ln\left(\frac{1}{S}\right) = \frac{1}{\tau} \times (t - t_0) \tag{S5}$$

where

$$S = 1 - \frac{V_b(t) - V_0}{\Delta V_b} \tag{S6}$$

S10. Responsivity of detector versus IR on/off period.

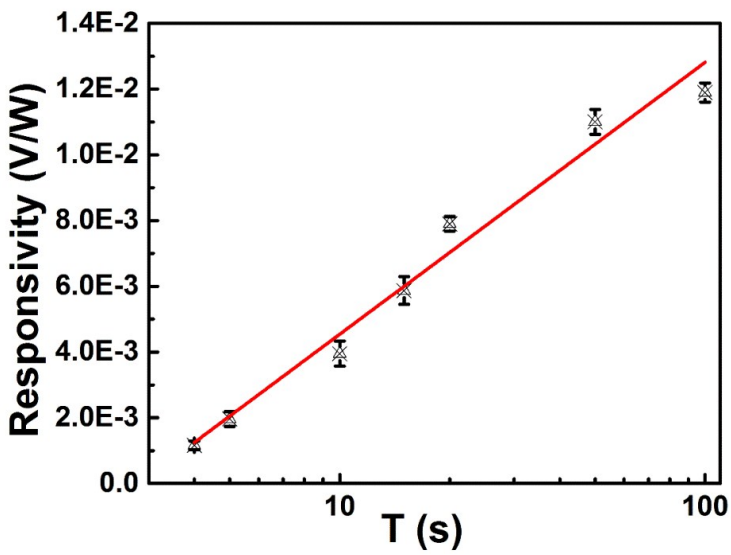

Fig. S10 Responsivity of detector versus IR on/off period

References

1. Q.-H. Yang, P.-X. Hou, M. Unno, S. Yamauchi, R. Saito and T. Kyotani, *Nano Lett.*, 2005, **5**, 2465-2469.
2. L. Bulusheva, A. Okotrub, I. Kinloch, I. Asanov, A. Kurenya, A. Kudashov, X. Chen and H. Song, *Phys. Status Solidi (b)*, 2008, **245**, 1971-1974.
3. D. J. Lipomi, M. Vosgueritchian, B. C. Tee, S. L. Hellstrom, J. A. Lee, C. H. Fox and Z. Bao, *Nat. Nanotechnolo.*, 2011, **6**, 788-792.
4. R. Martel, T. Schmidt, H. Shea, T. Hertel and P. Avouris, *Appl. Phys. Lett.*, 1998, **73**, 2447-2449.
5. V. Derenskyi, W. Gomulya, J. M. S. Rios, M. Fritsch, N. Fröhlich, S. Jung, S. Allard, S. Z. Bisri, P. Gordiichuk and A. Herrmann, *Adv. Mater.*, 2014, **26**, 5969-5975.
6. F. Xu, M.-Y. Wu, N. S. Safron, S. S. Roy, R. M. Jacobberger, D. J. Bindl, J.-H. Seo, T.-H. Chang, Z. Ma and M. S. Arnold, *Nano Lett.*, 2014, **14**, 682-686.
7. L. M. Ombaka, P. G. Ndungu and V. O. Nyamori, *RSC Adv.*, 2015, **5**, 109-112.
8. A. D. Franklin, *Nature*, 2013, **498**, 443-444.
9. R. H. Baughman, A. A. Zakhidov and W. A. de Heer, *Science*, 2002, **297**, 787-792.